Induced pluripotent stem cells derived brain endothelial cells from patients suffering from familial form of Alzheimer's disease display impaired barrier function and cell metabolism

Ronak Patel
Texas Tech University Health Sciences Center School of Pharmacy
Snehal Raut
Texas Tech University Health Sciences Center School of Pharmacy
Abraham Al-Ahmad (abraham.al-ahmad@ttuhsc.edu)
Texas Tech University Health Sciences Center https://orcid.org/0000-0001-7463-3204

Research

Keywords: iPSCs, blood-brain barrier, PSEN, familial form of Alzheimer's disease (FAD).

Posted Date: January 13th, 2020

DOI: https://doi.org/10.21203/rs.2.18501/v2

Version of Record: A version of this preprint was published on January 7th, 2021. See the published version at https://doi.org/10.1186/s12987-020-00235-y.

Abstract

Background: Alzheimer's disease (AD) is the most common most common form of neurodegenerative of neurodegenerative disease. It is an irreversible condition marked by irreversible cognitive loss, commonly attributed by the loss of hippocampal neurons due to the formation of senile plaques and neurofibrillary tangles. Although the sporadic form is the most prevalent, the presence of familial form (involving several genes such as APP, PSEN1 and PSEN2) of the disease is commonly used as a model for understanding the pathophysiology of the disease. The aim of this study is to investigate the effect of mutation on PSEN1 and PSEN2 genes on the BBB function using induced pluripotent stem cells (iPSCs) . Methods: iPSC lines from patients suffering from familial form of Alzheimer's diseases and harboring mutations in PSEN1 or PSEN2 were used in this study and compared to a control iPSC line. Cells were differentiated into brain microvascular endothelial cells (BMECs) following existing established differentiation protocols. Barrier function was assessed by measuring TEER and fluorescein permeability, drug transporters activity was assessed by uptake assay, glucose uptake and metabolism assessed by cell flux analyzer, mitochondrial potential by JC-1 and lysosomal acidification by acridine orange. Results: iPSC derived BMECs from the FAD patient presenting a mutation in PSEN1 gene PSEN1-BMECs, but not PSEN2-BMECs, showed impaired barrier function compared to the FAD patient harboring a mutation in PSEN2 and to control group. Such impaired barrier function correlated with poor tight junction complexes and reduced drug efflux pump activity. In addition, both PSEN1 and PSEN2 -BMECs displayed reduced glucose uptake and glycolysis, as well as impaired mitochondrial membrane potential and lysosomal acidification. Conclusion: Our study reports evidence that PSEN1 and PSEN2 mutations, two genes commonly associated with familial form of Alzheimer's disease that iPSC -derived BMECs obtained from FAD patients showed impaired barrier properties and BMECs metabolism. In particular, PSEN1 mutation was associated with a more detrimental phenotype than the PSEN2 mutation, as noted by a reduced barrier function, reduced drug efflux pump activity and diminished glucose metabolism . , can impair the development and the maintenance of the BBB, both by an impairement of the barrier function, vesicle trafficking and bioenergetics. Therefore, assessing the contribution of genetic mutations associated with Alzheimer's disease will allow us to better understand the contribution of the BBB in dementia, but also in other neurodegenerative diseases.

Background

Alzheimer's disease (AD) is the most common form of dementia. It is a progressive and incurable neurodegenerative disease accounting as the 6th cause of death in the United States. It is estimated that over 10% of the US senior population is diagnosed with AD (1).

The pathophysiology of the disease remains unclear, however it is characterized by several features including the formation of amyloid plaques (rich in Ab peptides) (2, 3) and hyperphosphorylation of Tau protein in the hippocampus region (4-7), resulting in neuronal cell death and ultimately propagating to the cortical regions surrounding the hippocampus. These two features provide sources for two hypotheses (the Ab hypothesis and the Tau hypothesis respectively) that have been used as potential target for the

development of therapies. Despite the important effort aimed to find a cure for such disease and the development of various animal models of the disease (including transgenic mice), translation from pre-clinical models into clinically relevant therapies remains the main pitfall in such effort (8, 9).

Recently, the use of induced pluripotent stem cells (iPSCs) as a tool to model Alzheimer's disease (AD) has recently gained attraction (10-12). Interestingly, such iPSCs are derived from patients suffering from familial form of AD (FAD), characterized by mutations in genes associated with AD including amyloid precursor protein (APP) or presenilin (PSEN1, PSEN2).Although the pathogenesis of AD has been primarily focused on a neurocentric approach, recent studies have suggested the contribution of non-neuronal cells into the pathophysiology, including the blood-brain barrier (BBB).

Several studies by Zlokovic and colleagues have demonstrated a contribution of the BBB into the pathophysiology of AD (13-18). In a recent review, Montagne and colleagues reported several in vivo studies performed in PSEN1 transgenic mice, such animals displayed signs of an impaired barrier function in the form of microhemorrhage and increased permeability to tracers and large proteins (albumin, fibrin, IgG) (19). Yet, the presence of similar features at the BBB of FAD patients harboring such mutations in the PSEN genes remains to be documented. The aim of this study is to document the effect of mutations in PSEN1 and PSEN2 genes on the barrier function using iPSCs derived from patients suffering from FAD (12, 20, 21). Using the differentiation protocol initially developed by Shusta and colleagues (22, 23), this study investigated the effect of mutations on PSEN1 and PSEN2 genes on the barrier phenotype in iPSC-derived brain microvascular cells (BMECs).

Materials And Methods

Cell culture and iPSC differentiation

Control (CS06iCTR), PSEN1 (CS40iFAD) and PSEN2 (CS08iFAD) iPSC lines used in this study were acquired from the Cedars-Sinai iPSC core (Los Angeles, CA). The PSEN1 iPSC line was isolated from a 56-year old Caucasian male diagnosed with memory impairment and harbors an Ala246Glu mutation. The PSEN2 iPSC line was isolated from an 81-year old Caucasian female diagnosed with progressive dementia and harbors an Asn141Ile mutation.

Undifferentiated iPSCs were maintained in hESC-grade Matrigel® (Corning, Corning, NY) in presence of Essential 8 (E8) medium (Life Technologies, ThermoFisher, Waltham, MA) as previously described (24). iPSC differentiation into BMECs occurred following the differentiation protocol previously published by our lab (24). Briefly, cells were maintained in E8 for 5 days prior to differentiation, followed by 6 days in unconditioned medium [UM: Dulbecco's modified Eagle's medium/F12 with 15 mM HEPES (ThermoFisher), 20% knockout serum replacement (ThermoFisher), 1% non-essential amino acids (ThermoFisher), 0.5% Glutamax (ThermoFisher), and 0.1 mM b-mercaptoethanol (Sigma-Aldrich, St. Louis, MO, USA)] and 2 days 2 days in EC+/+ [EC medium (ThermoFisher) supplemented with 1% platelet-poor derived serum (PDS, Alfa-Aesar, ThermoFisher, Haverhill, MA, USA), 20 ng/mL human recombinant basic fibroblast growth factor (Tocris, Abingdon, UK), and 10 µM retinoic acid (Sigma-Aldrich)]. At day 8

of differentiation, cells were enzymatically dissociated (Accutase®, Corning) and seeded on tissue culture plastic surfaces (TCPS) coated with collagen (isolated from human placenta, Sigma-Aldrich)/fibronectin (bovine plasma, Sigma-Aldrich) at concentrations of 80 µg/cm2 and 20 µg/cm^2 respectively. At day 9 of differentiation, iPSC-derived BMECs were maintained in EC-/- medium [EC medium supplemented with 1% PDS] for 24 hours. Experiments were conducted at day 10 of differentiation.

Immunofluorescence

Cells were quickly washed with ice-cold PBS and fixed in 4% paraformaldehyde (PFA, Electron Microscopy Sciences, Hatfield, PA, USA) and blocked for 30 minutes at room temperature (RT) in presence of PBS supplemented with 10% goat serum (ThermoFisher) supplemented with 0.2% Triton-X100 (Sigma). Cells were incubated overnight at 4ºC in primary antibodies targeting BCRP (1:100, Millipore, RRID: AB_11213795), claudin-5 (1:100, Life Technologies, RRID: AB_2533200), GLUT1 (1:100, ThermoFisher, AB_10979643), GLUT3 (1:100, ThermoFisher, AB_2809974), GLUT4 (1:100, ThermoFisher, AB_11153908), MRP1 (1:100, Millipore, RRID: AB_2143819), occludin (1:100, Life Technologies, AB_2533101) and P-gp (1:50, ThermoFisher, AB_1233253) diluted in 10% goat serum (PBSG). Primary antibodies detection occurred by incubation with goat-anti mouse Alexa Fluor® 555-conjugated secondary goat anti-mouse (Life Technologies) for 1 hour at room temperature. Cells were observed at 200X magnification (20X long-distance dry objective) and acquired using a Leica DMi-8 inverted epifluorescence microscope (Leica Microsystems, Wetzlar, Germany). Images were processed using ImageJ (Image J, NIH, Bethesda, MD). Relative fluorescence was quantified using the built-in function in ImageJ. Background fluorescence was subtracted from unlabeled cells incubated with the secondary antibody only.

TEER and permeability experiments

Barrier tightness was measured by assessing both transcellular electrical resistance (TEER) and fluorescein permeability (paracellular tracer). TEER was measured using an EVOHM STX2 chopstick electrode (World Precision Instruments, Sarasota, FL, USA). For each experiment, three measurements were performed for each insert, and the average resistance obtained was used to determine barrier function. Fluorescein permeability was assessed by incubating 10 µM sodium fluorescein (Sigma-Aldrich) in the donor (apical) chamber, with sampling in the donor (basolateral) chamber every 15 minutes for up to 60 minutes. Fluorescein permeability (P_e) was calculated using the clearance slopes obtained by extrapolation using the following formula:

P_t and P_f indicative of the clearance slopes of samples and blank (empty coated) filters, and S indicative of the insert surface area (cm^2).

Drug uptake assay

Cells were incubated in the presence of 10μM Rhodamine 123 (P-gp substrate, Sigma), FL-BOPIDY (BCRP substrate, Sigma) or CM-DCFDA (MRP substrate, Sigma) for 1 hour at 37ºC followed by cell lysis using RIPA buffer (ThermoFisher). For assessing the contribution of efflux pump in the drug uptake, cells were pre-incubated for 1 hour in presence of 5μM cyclosporine A (CsA, P-gp inhibitor, Sigma), 1μM Ko143 (BCRP inhibitor, Sigma) or 10μM MK571 (MRPs inhibitor, Sigma) and maintained during the incubation with drug efflux substrate. Following incubation, cells were briefly washed with ice-cold PBS and lysed with RIPA buffer. Fluorescence in cell lysates was assessed using a SynergyMX^2 ELISA plate reader (Bio-Tek, Winooski, VT, USA). Relative fluorescence units (RFU) were normalized against the total protein content and the protein levels were determined by bicinchoninic acid assay (BCA, ThermoFisher). Fluorescence values (expressed as relative fluorescence unit or RFU) obtained from cell lysates in the absence of inhibitor (named as controls) were normalized to the protein content and expressed as RFU/μg protein.

Glucose uptake assay

Cells were incubated in presence of [^{14}C]-D-glucose (0.4μCi/mL) for 1 hour at 37ºC.

Following incubation, cells were briefly washed with ice-cold PBS and lysed with RIPA buffer. In experiments involving GLUT1 inhibition, cells were pre-incubated in presence of 10μM glucose transporter inhibitor II (Millipore-Sigma, Danvers, MA) for 1 hour prior incubation with glucose. Radioactivity in cell lysates was assessed using liquid scintillation cocktail (Scintisafe® 30%, ThermoFisher) and quantified with a Beckman-Coulter LS6500 (Beckman-Coulter, Brea, CA). Glucose uptake levels were normalized by the total amount of protein in samples.

Glycolytic flux analysis

Glycolytic flux analysis was assessed using a Seahorse Xf24 cell flux analyzer (Agilent Technologies, Santa Clara, CA). Cells were seeded on custom-designed 24-well plates (Agilent Technologies) at day 8 of differentiation and allowed to grow for 48 hours. On the day of experiments, cell medium was replaced by glucose-free medium provided with the glycolytic stress test kit (Agilent) for 2 hours prior experiment. Cell medium was replaced once with glucose-free medium and initiated measurement. At 20 minutes of incubation, 10mM D-glucose was added in the incubation chamber, followed by the addition of 1μM of oligomycin at 40 minutes and finally addition of 100mM 2-deoxy-D-glucose (2-DG) at 60 minutes timepoint, with measurements occurring until the 90th minute timepoint.

Flow cytometry

At day 10 of differentiation, cells were enzymatically dissociated with Accutase®. Cells were resuspended and centrifuged and resuspended in medium containing 5µM JC-1 dye (ThermoFisher) for 30 minutes at 37ºC. In experiments involving FCCP treatment, cells were simultaneously treated with 50nM FCCP. Following incubation with JC-1 dye, cells were washed by centrifugation and resuspension in 200µL PBS for flow cytometry analysis. In experiments involving acridine orange (AO), cells were maintained for 24 hours in EC-/- medium or in serum-free EC medium to induce serum starvation. Following such treatment, cells were centrifuged and stained with 1µg/mL acridine orange (AO, Sigma-Aldrich) dissolved in PBS and allowed to stain for 15 minutes, following the protocol of Thome and colleagues (25). Fluorescence detection in samples were performed using a FACSVerse® flow cytometer (BD Biosciences, San Jose, CA). Fluorescence PMTs were calibrated on unstained cells and set for the remaining of the experiments.

Lysosensor cell imaging

Live cells were incubated in presence of 1µM Lysosensor-Green DND 189 for 5 minutes, followed by a brief wash with ice-cold PBS and fixation with 4% paraformaldehyde. Cells were counterstained with 300nM DAPI solution and immediately processed for imaging under the Leica DMi-8 inverted fluorescence microscope at 20X.

Statistics

Data are represented as mean ± S.D. from at least three independent experiments. Statistical analysis was performed using one-way analysis of the variance (ANOVA) using parametric (Dunnett) tests. Statistical analysis was performed using GraphPad Prism 8.0

(GraphPad Software, La Jolla, CA). A p-value lesser than 0.05 ($P<0.05$) was considered as indicative of a statistic difference between one or more groups.

Results

BMECs from PSEN1 patient showed impaired barrier function

The first goal of this study aimed to assess the presence of a BMEC phenotype in iPSC derived BMECs from FAD patients compared to control iPSCs (Figure 1). Thus, the expression of cell markers associated with BMECs were assessed using immunocytochemistry (Fig.1A). Interestingly, PSEN1-BMECs displayed a lower immunoreactivity to claudin-5 and occludin (Fig.1A), such lower immunoreactivity was further

confirmed by quantification of protein expression by fluorescence intensity (Fig.1B). PSEN1-BMECs displayed overall lower expression of these two tight junction (TJ) proteins, whereas PSEN2-BMECs showed no differences to the control iPSC line. The expression pattern of these TJ proteins was comparable to other iPSC lines obtained from control (healthy) patients (24). To better correlate the deficiency in the expression of TJ complexes with an impaired barrier function, changes in TEER and fluorescein permeability were measured in all three cell lines (Fig.1C&D). PSEN1-BMECs showed impaired barrier function compared to the two other iPSC lines, as a significantly lower TEER (150 Ω.cm^2) and higher fluorescein permeability. In the other hand, TEER and permeability values reported in the control and PSEN2-BMECs were comparable to control iPSC lines previously used by our group (24), as these monolayers displayed tight monolayers (>1000 W.cm^2) and low paracellular permeability to fluorescein (10e-5cm/min). Such impaired phenotype appeared not limited to BMECs, as iPSC-derived neurons originated from PSEN1 iPSCs displayed an impaired formation of maturing neurons as represented by formation of neurites compared to control and PSEN2-neurons (Supplementary Figure 1). Taken together our data suggests that PSEN1, but in lesser extent PSEN2, may impair the barrier function in BMECs.

PSEN1-BMECs have impaired drug efflux pumps activity

To further investigate the BMEC phenotype associated with FAD, changes in ABC transporters expression (by immunocytochemistry) and activity (by drug uptake assay) were documented in this study (Figure 2). All three iPSC derived BMECs displayed the expression of common ABC transporters expressed at the BBB (Fig.2A), including ABCB1 (P-gp), ABCC1 (MRP1) and ABCG2 (BCRP). No significant differences were observed in the relative expression of these transporters, albeit ABCB1 and ABCC1 displayed a slightly lower immunoreactivity in PSEN1-BMECs. To further investigate the possible differences in drug efflux pump activity between the different iPSC lines used, fluorescence substrate uptake assays were performed in all three cell lines. PSEN1-BMECs showed higher drug uptake levels for rhodamine-123 (Fig.2B, a P-gp substrate) and DCFDA (Fig.2C, an MRPs substrate), and confirmed by the relative absence of change in cellular uptake following treatment with cyclosporine A (CsA, a P-gp inhibitor) or MK571 (a pan-MRP inhibitor). In contrast, no significant differences were observed in regards of BCRP activity. In conclusion, mutation in the PSEN1 gene may impair the activity of certain drug efflux transporters.

PSEN1 and PSEN2-BMECs display impaired glucose uptake and metabolism

Next, changes in glucose uptake and metabolism between iPSC lines were assessed (Figure 3). No significant changes in glucose transporter isoforms (GLUT1, GLUT3, GLUT4) at the BBB were observed (Fig.3A). However, PSEN1-derived BMECs showed a lower glucose uptake (Fig.3B) compared to controls and PSEN2-BMECs. Although PSEN2-BMECs showed similar glucose uptake than controls, these cells still showed a slight decrease compared to control. In addition, both PSEN1-BMECs and PSEN2-BMECs failed to show inhibition of glucose uptake following treatment with glucose transporter inhibitor II (GTI). Notably, similar pattern was observed with iPSC-astrocytes (Supplementary Figure 2), as PSEN1-

astrocytes showed lower glucose uptake than control-astrocytes. However, all three groups showed significant decrease in glucose uptake following treatment with GTI. To investigate the impact of such impaired glucose uptake on the cell metabolism, we investigated changes in glycolysis in iPSC derived BMECs using a cell flux analyzer (Fig.3D). Both PSEN1-BMECs and PSEN2-BMECs showed a basal extracellular acidification rate (ECAR) compared to control-BMECs. Both PSEN-BMECs showed a metabolic phenotype considered “quiescent”, compared to a “glycolytic” phenotype observed with control-BMECs. A detailed analysis of the glycolytic stress assay showed a decrease in glycolysis and non-glycolytic activity only in PSEN1-BMECs, whereas a decreased glycolytic capacity and glycolytic reserve were observed in both PSEN-BMECs. In conclusion, mutations in PSEN genes maybe impairing glucose uptake and metabolism at the BBB.

PSEN1 mutation impairs mitochondrial and lysosomal acidification

PSENs are commonly associated with their function within the g-secretase complex. However, recent studies highlighted the contribution of PSENs to other biological functions, including autophagy and mitophagy (26-28). In particular, mutations in PSENs have been documented to be associated with impaired mitochondrial Ca2+ homeostasis and impaired mitochondrial function (29, 30). Therefore, we investigated changes in the mitochondrial function and autophagy in iPSC derived BMECs (Fig.4) to report similar outcomes than reported in the literature in non-endothelial cells. Firstly, changes in cell metabolic activity were assessed in iPSC-BMECs monolayers using an MTS assay (Fig.4A). Interestingly, PSEN1-BMECs showed a higher cell metabolic activity than control and PSEN2-BMECs, suggesting a higher proliferation rate. Similar outcomes in terms of MTS levels was observed in iPSC-derived neurons (Supplementary Figure 2B), whereas no differences in iPSC-derived astrocytes was reported. To confirm if such differences in cell metabolic activity were due to changes in mitochondrial potential, changes in JC-1 fluorescence profile (Fig.4B). Under resting condition, control BMECs showed most cell events as high “red” (PE emission filter) fluorescence and low “green” (FITC emission filter) , suggesting the presence of a mitochondrial membrane potential. Following treatment with CCCP (a mitochondria uncoupler), JC-1 fluorescence emission shifted from “red” to “green” wavelength, with the majority of cell events reported in the control iPSC line occurred in the “green” emission filter. In contrast, PSEN1-BMECs and PSEN2-BMECs showed an overall lower “red” fluorescence and higher “green” intensity compared to control, suggesting a possible impairment in the mitochondrial membrane potential. Treatment with CCCP failed to fully shift the cell events towards the “green” filter, further evocating a possible impairment in the mitochondria cell membrane potential.

As mutations in PSEN1 correlated with impaired mitophagy in vitro and in vivo in non-BMECs cells, we investigated the possible impairment of cell autophagy in FAD cells, using Lysosensor® Green and Acridine Orange (AO), as fluorescent dyes indicative of change in lysosomal pH (Fig.4C&D respectively). Control BMECs displayed presence of dense green peri-nuclear punctate indicative of acidified lysosomes. In contrast, the lack of Lysosensor® Green punctate in PSEN1-BMECs was indicative of weak lysosomal acidification. PSEN2-BMECs appeared similar to control BMECs.

To confirm the impaired lysosomal acidification observed in PSEN1-BMECs following treatment with Lysosensor® Green, cells were treated with AO and quantified using flow cytometry (Fig.4D). Control-BMECs were characterized by the presence of predominant high “red” (emission in PerCP filter) /high "green” (emission in FITC filter) cellular events. Such feature is commonly accepted as indicative of acidic lysosomes (25). In contrast, PSEN1-BMECs showed a notable decrease in acidic lysosomes compared to control-BMECs, as the majority of such events recorded as low “red”/high “green” events. PSEN2-BMECs showed an intermediate pattern, as a tail in low “red”/low “green” quadrant was observed.

Induction of autophagy by serum starvation triggered a shift from “green” to “red” fluorescence, suggestive of an increase in acidic vesicular organelles (AVOs), as reported by Thome and colleagues (25). Such increase was reported in all three groups. In summary, FAD-associated mutations may impair mitochondrial membrane potentials and autophagy in BMECs.

Discussion

Alzheimer’s disease (AD) is the most common form of dementia and represents the 6th cause of death in the United States. Because aging is the first risk factor by its preponderance, the increase of its occurrence amongst an aging population raises an important public health issue. Several studies highlighted the contribution of genetic mutations in presenilin genes (PSEN1, PSEN2) as element of AD pathophysiology, as well as a possible association between PSEN1 mutations and disruption of the BBB integrity in vivo (19). Yet, the evidence of an impaired barrier function at the human BBB in patients harboring mutations in PSENs remains unknown. In this study, using iPSCs derived from patients suffering from FAD, we investigated the possible link between PSENs and impaired barrier function. This study suggests that mutations in the PSEN1 gene may be detrimental on the barrier function, as we reported a worsened barrier tightness in BMECs, decreased glucose uptake and metabolism and impaired mitochondrial membrane potential. Such findings seems to correlate with a recent study by Searson and colleagues using an iPSC line sharing the same mutation in PSEN1 (31). Our study is in agreement with this study, as we both observed that PSEN1-BMECs BMECs showed poor barrier function (as measured by TEER and permeability with a paracellular marker) compared to control BMECs. Furthermore, our group showed that MRP-mediated efflux in PSEN1-BMECs was also affected, as well as glucose metabolism (glucose uptake, glycolysis), as well as glucose metabolism, mitochondrial function and lysosomal acidification. Although our study highlighted such dramatic changes in PSEN1, we cannot exclude that similar outcomes may occur in PSEN2 BMECs as well, albeit in a much slower rate. Therefore, further investigations comparing PSEN1 and PSEN2 mutations and their effects on the BBB (using both in vitro and in vivo models) could provide some insights on the contribution of PSEN1 and PSEN2 mutations effects on the BBB function.

A major limitation of this study is highlighted by the limited number of FAD iPSC lines available from patients in public repositories. Because of such limitations, we cannot completely exclude that the impairment observed in the PSEN1 iPSC line maybe inherent to the iPSC clone used in this study, although our findings aligned with the existing literature (31). Hence, our future goal is to confirm these

initial findings by the inclusion of additional iPSC lines from patients harboring mutations in both PSEN1 and PSEN2 lines.

A particular feature observed in our study was the lower glucose uptake in both PSEN1 and PSEN2 iPSC lines compared to control. Such lower uptake was accompanied by a lack of response to GLUT inhibition by GTI, and by a much lower ECAR values and glycolytic capacity compared to controls. Although the overall expression of GLUT1 appeared unchanged, we cannot exclude a possible impaired GLUT1 activity due to intrinsic factor. GLUT1 has been documented to have a particular interactions with Ab, as a recent study by Zlokovic and colleagues reported a worsened outcome in AD transgenic mice crossed with Slc2a1+/- deficient mice (15). Hence, our future direction will be to further investigate the relationships and interactions between Ab peptides and GLUT1.

The effect of PSEN1 and PSEN2 on the BBB maturation and maintenance is intriguing. Both proteins are known to be part of the g-secretase complex, which ultimately drives the formation of Ab peptides. Therefore, assessing the secretion of Ab peptides by these cell lines, and comparing such secretion levels to primary human BMECs, would further advance our understanding the effect of Ab peptides on the BBB integrity.

In addition, g-secretase has been documented as an important modulator of the canonical WNT signaling pathway (32, 33). WNT signaling is an important pathway involved in the development and maintenance of the BBB (34, 35). At this point, we cannot restrict and determine if the impairment of the BBB by PSEN1 is driven by an increase in Ab production, or by an impairment of the endogenous WNT signaling. A limitation of our study is the absence of documentation of Ab1-40 and Ab1-42 production by our BMECs monolayers. Assessing differential secretion of these Ab peptides between PSEN mutants and control iPSC lines could help us better understand the contribution of each of these pathways on the BBB. Finally, we have reported an impaired mitochondrial function (as seen by JC-1 staining) and lysosomal acidification. These are two components playing essential roles in the maintenance of energy homeostasis as well as vesicular trafficking. These two features remain largely undocumented at the BBB despite their important contribution in neurological diseases. Thus, a better understanding on how PSENs impact these pathways may increase interest in understanding the contribution of these pathways on the BBB dysfunction during neurological diseases.

Conclusion

In conclusion, this study suggests the importance of PSEN1 on the BBB development and maturation, as mutation in PSEN1 appears to have detrimental effect on the BBB function. Such study raises the importance to investigate the contribution of genetic disorders at the BBB, and the possible inclusion of a dysfunctional BBB in the pathophysiology of the disease.

Declarations

Availability of data and materials

The data presented in this work is available upon request.

Ethics approval and consent to participate

The acquisition of such unidentified cell lines was approved by the institutional biosafety committee and in compliance with the institutional research integrity office. Consent for publication was not applicable.

Competing interests

The authors have no conflicts to disclose.

Funding information

This study was funded by TTUHSC institutional funds to AA.

Authors' contributions

RP and SR have performed the experiments and analyzed the data. AA designed the experiments and redacted the manuscript.

References

1. Hebert LE, Weuve J, Scherr PA, Evans DA. Alzheimer disease in the United States (2010-2050) estimated using the 2010 census. Neurology. 2013;80(19):1778-83.
2. Mehta PD, Pirttila T, Patrick BA, Barshatzky M, Mehta SP. Amyloid beta protein 1-40 and 1-42 levels in matched cerebrospinal fluid and plasma from patients with Alzheimer disease. Neurosci Lett. 2001;304(1-2):102-6.
3. Selkoe DJ, Hardy J. The amyloid hypothesis of Alzheimer's disease at 25 years. EMBO Mol Med. 2016;8(6):595-608.
4. Alonso AD, Beharry C, Corbo CP, Cohen LS. Molecular mechanism of prion-like tau-induced neurodegeneration. Alzheimers Dement. 2016;12(10):1090-7.
5. Chong FP, Ng KY, Koh RY, Chye SM. Tau Proteins and Tauopathies in Alzheimer's Disease. Cell Mol Neurobiol. 2018;38(5):965-80.
6. Dorszewska J, Prendecki M, Oczkowska A, Dezor M, Kozubski W. Molecular Basis of Familial and Sporadic Alzheimer's Disease. Curr Alzheimer Res. 2016;13(9):952-63.
7. Garcia-Leon JA, Cabrera-Socorro A, Eggermont K, Swijsen A, Terryn J, Fazal R, et al. Generation of a human induced pluripotent stem cell-based model for tauopathies combining three microtubule-

associated protein TAU mutations which displays several phenotypes linked to neurodegeneration. Alzheimers Dement. 2018;14(10):1261-80.

8. Braidy N, Munoz P, Palacios AG, Castellano-Gonzalez G, Inestrosa NC, Chung RS, et al. Recent rodent models for Alzheimer's disease: clinical implications and basic research. J Neural Transm (Vienna). 2012;119(2):173-95.
9. Cummings JL, Morstorf T, Zhong K. Alzheimer's disease drug-development pipeline: few candidates, frequent failures. Alzheimers Res Ther. 2014;6(4):37.
10. Jung YW, Hysolli E, Kim KY, Tanaka Y, Park IH. Human induced pluripotent stem cells and neurodegenerative disease: prospects for novel therapies. Curr Opin Neurol. 2012;25(2):125-30.
11. Mohamet L, Miazga NJ, Ward CM. Familial Alzheimer's disease modelling using induced pluripotent stem cell technology. World journal of stem cells. 2014;6(2):239-47.
12. Yagi T, Ito D, Okada Y, Akamatsu W, Nihei Y, Yoshizaki T, et al. Modeling familial Alzheimer's disease with induced pluripotent stem cells. Hum Mol Genet. 2011;20(23):4530-9.
13. Sweeney MD, Montagne A, Sagare AP, Nation DA, Schneider LS, Chui HC, et al. Vascular dysfunction-The disregarded partner of Alzheimer's disease. Alzheimers Dement. 2019;15(1):158-67.
14. Zhao Z, Sagare AP, Ma Q, Halliday MR, Kong P, Kisler K, et al. Central role for PICALM in amyloid-beta blood-brain barrier transcytosis and clearance. Nat Neurosci. 2015;18(7):978-87.
15. Winkler EA, Nishida Y, Sagare AP, Rege SV, Bell RD, Perlmutter D, et al. GLUT1 reductions exacerbate Alzheimer's disease vasculo-neuronal dysfunction and degeneration. Nat Neurosci. 2015;18(4):521-30.
16. Tarasoff-Conway JM, Carare RO, Osorio RS, Glodzik L, Butler T, Fieremans E, et al. Clearance systems in the brain-implications for Alzheimer disease. Nat Rev Neurol. 2015;11(8):457-70.
17. Sagare AP, Bell RD, Zhao Z, Ma Q, Winkler EA, Ramanathan A, et al. Pericyte loss influences Alzheimer-like neurodegeneration in mice. Nat Commun. 2013;4:2932.
18. Zlokovic BV. Neurovascular pathways to neurodegeneration in Alzheimer's disease and other disorders. Nat Rev Neurosci. 2011;12(12):723-38.
19. Montagne A, Zhao Z, Zlokovic BV. Alzheimer's disease: A matter of blood-brain barrier dysfunction? J Exp Med. 2017;214(11):3151-69.
20. Yankner BA, Duffy LK, Kirschner DA. Neurotrophic and neurotoxic effects of amyloid beta protein: reversal by tachykinin neuropeptides. Science. 1990;250(4978):279-82.
21. Do Carmo S, Cuello AC. Modeling Alzheimer's disease in transgenic rats. Mol Neurodegener. 2013;8(1):37.
22. Lippmann ES, Al-Ahmad A, Azarin SM, Palecek SP, Shusta EV. A retinoic acid-enhanced, multicellular human blood-brain barrier model derived from stem cell sources. Sci Rep. 2014;4:4160.
23. Lippmann ES, Azarin SM, Kay JE, Nessler RA, Wilson HK, Al-Ahmad A, et al. Derivation of blood-brain barrier endothelial cells from human pluripotent stem cells. Nat Biotechnol. 2012;30(8):783-91.

24. Patel R, Page S, Al-Ahmad AJ. Isogenic blood-brain barrier models based on patient-derived stem cells display inter-individual differences in cell maturation and functionality. J Neurochem. 2017;142(1):74-88.
25. Thome MP, Filippi-Chiela EC, Villodre ES, Migliavaca CB, Onzi GR, Felipe KB, et al. Ratiometric analysis of Acridine Orange staining in the study of acidic organelles and autophagy. J Cell Sci. 2016;129(24):4622-32.
26. Checler F, Goiran T, Alves da Costa C. Presenilins at the crossroad of a functional interplay between PARK2/PARKIN and PINK1 to control mitophagy: Implication for neurodegenerative diseases. Autophagy. 2017;13(11):2004-5.
27. Martin-Maestro P, Sproul A, Martinez H, Paquet D, Gerges M, Noggle S, et al. Autophagy Induction by Bexarotene Promotes Mitophagy in Presenilin 1 Familial Alzheimer's Disease iPSC-Derived Neural Stem Cells. Mol Neurobiol. 2019;56(12):8220-36.
28. Fedeli C, Filadi R, Rossi A, Mammucari C, Pizzo P. PSEN2 (presenilin 2) mutants linked to familial Alzheimer disease impair autophagy by altering Ca(2+) homeostasis. Autophagy. 2019;15(12):2044-62.
29. Sarasija S, Norman KR. A gamma-Secretase Independent Role for Presenilin in Calcium Homeostasis Impacts Mitochondrial Function and Morphology in Caenorhabditis elegans. Genetics. 2015;201(4):1453-66.
30. Sarasija S, Laboy JT, Ashkavand Z, Bonner J, Tang Y, Norman KR. Presenilin mutations deregulate mitochondrial Ca(2+) homeostasis and metabolic activity causing neurodegeneration in Caenorhabditis elegans. Elife. 2018;7.
31. Katt ME, Mayo LN, Ellis SE, Mahairaki V, Rothstein JD, Cheng L, et al. The role of mutations associated with familial neurodegenerative disorders on blood-brain barrier function in an iPSC model. Fluids Barriers CNS. 2019;16(1):20.
32. Yang J, Zhao H, Ma Y, Shi G, Song J, Tang Y, et al. Early pathogenic event of Alzheimer's disease documented in iPSCs from patients with PSEN1 mutations. Oncotarget. 2017;8(5):7900-13.
33. Van Gassen G, De Jonghe C, Nishimura M, Yu G, Kuhn S, St George-Hyslop P, et al. Evidence that the beta-catenin nuclear translocation assay allows for measuring presenilin 1 dysfunction. Mol Med. 2000;6(7):570-80.
34. Daneman R, Agalliu D, Zhou L, Kuhnert F, Kuo CJ, Barres BA. Wnt/beta-catenin signaling is required for CNS, but not non-CNS, angiogenesis. Proceedings of the National Academy of Sciences of the United States of America. 2009;106(2):641-6.
35. Liebner S, Corada M, Bangsow T, Babbage J, Taddei A, Czupalla CJ, et al. Wnt/beta-catenin signaling controls development of the blood-brain barrier. J Cell Biol. 2008;183(3):409-17.
36. Martinez A, Al-Ahmad AJ. Effects of glyphosate and aminomethylphosphonic acid on an isogeneic model of the human blood-brain barrier. Toxicol Lett. 2019;304:39-49.

Supplementary Figures

Supplementary Figure 1: Phenotype of iPSC-derived neurons differentiated from the iPSC lines. Cells were differentiated into neurons following existing protocol (24, 36). Neurons were stained against nestin (red), bIII-tubulin. DAPI was used as nuclear counterstaining.

Supplementary Figure 2: Effect of PSEN1 and PSEN2 mutations on astrocytes glucose uptake and cell metabolic activity. (A) Glucose uptake assay in iPSC-derived astrocytes. Note the similar decrease in glucose uptake as observed in BMECs. Note the efficacy of GTI as a pharmacological inhibitor for GLUTs, as all three cell lines showed a significant decrease in glucose uptake. (B) Cell metabolic activity in astrocytes and neurons using an MTS-assay. Note the higher cell metabolic activity reported in PSEN1-neurons compared to other groups, such higher metabolic rate being absent in astrocytes.

Figures

Figure 1

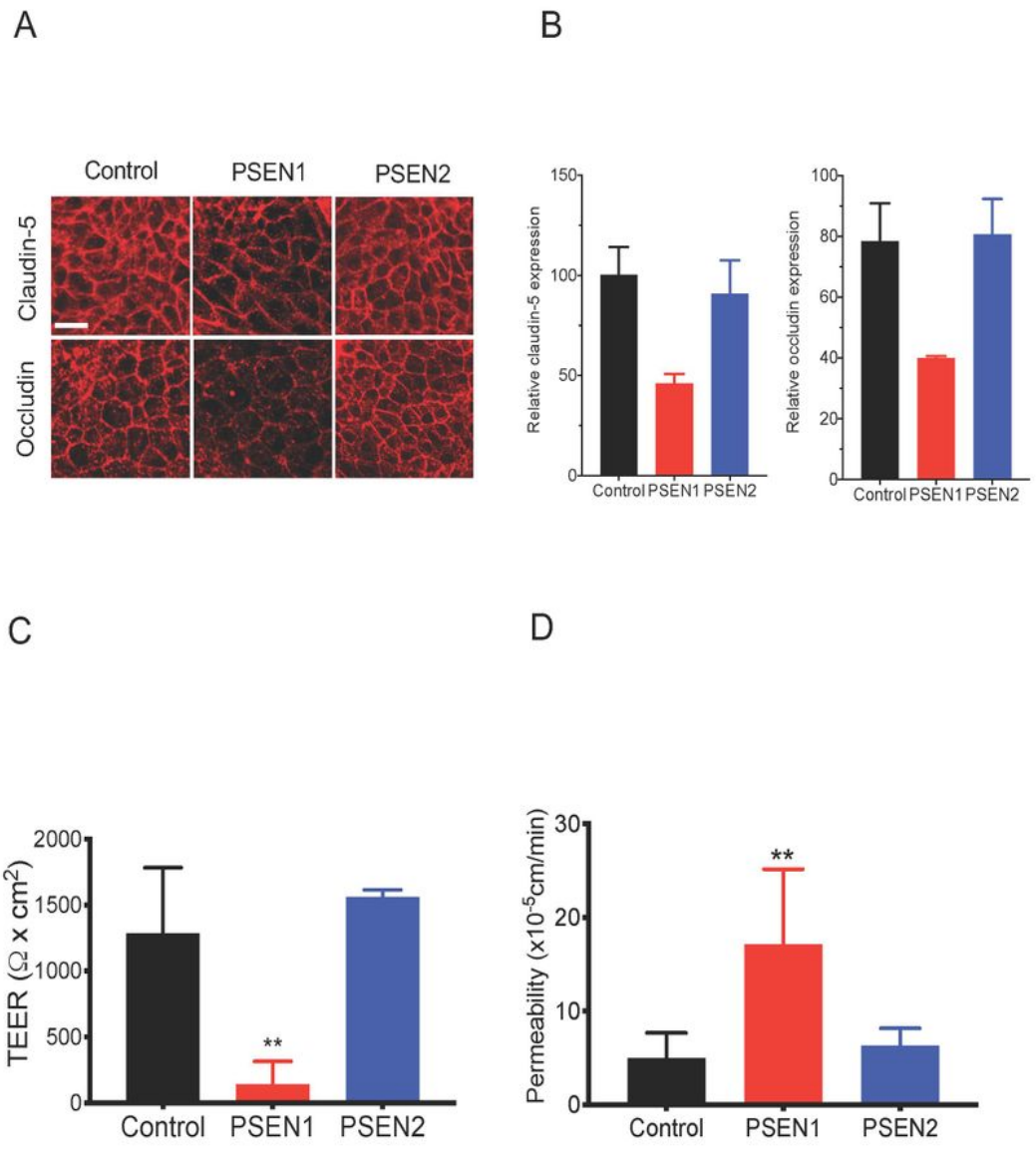

Figure 1

PSEN2-BMECs show impaired tight junctions and barrier function. (A) Representative micrograph picture of claudin-5 and occludin immunofluorescence in iPSC-derived BMECs differentiated from control, PSEN1 and PSEN2 patients. Scale bar = 50 µm. (B) Semi-quantitative analysis of claudin-5 and occludin protein expression. Protein expression was quantified using fluorescence intensity obtained in random fields. Note the relative lower expression of claudin-5 and occludin in PSEN1 group compared to PSEN2 group.

(C) TEER and (D) fluorescein permeability values in iPSC-derived BMECs at day 10 of differentiation. Note the poor TEER value and higher permeability in PSEN1 group compared to other groups. N=3/group, ** denotes P<0.01 compared to controls.

Figure 2

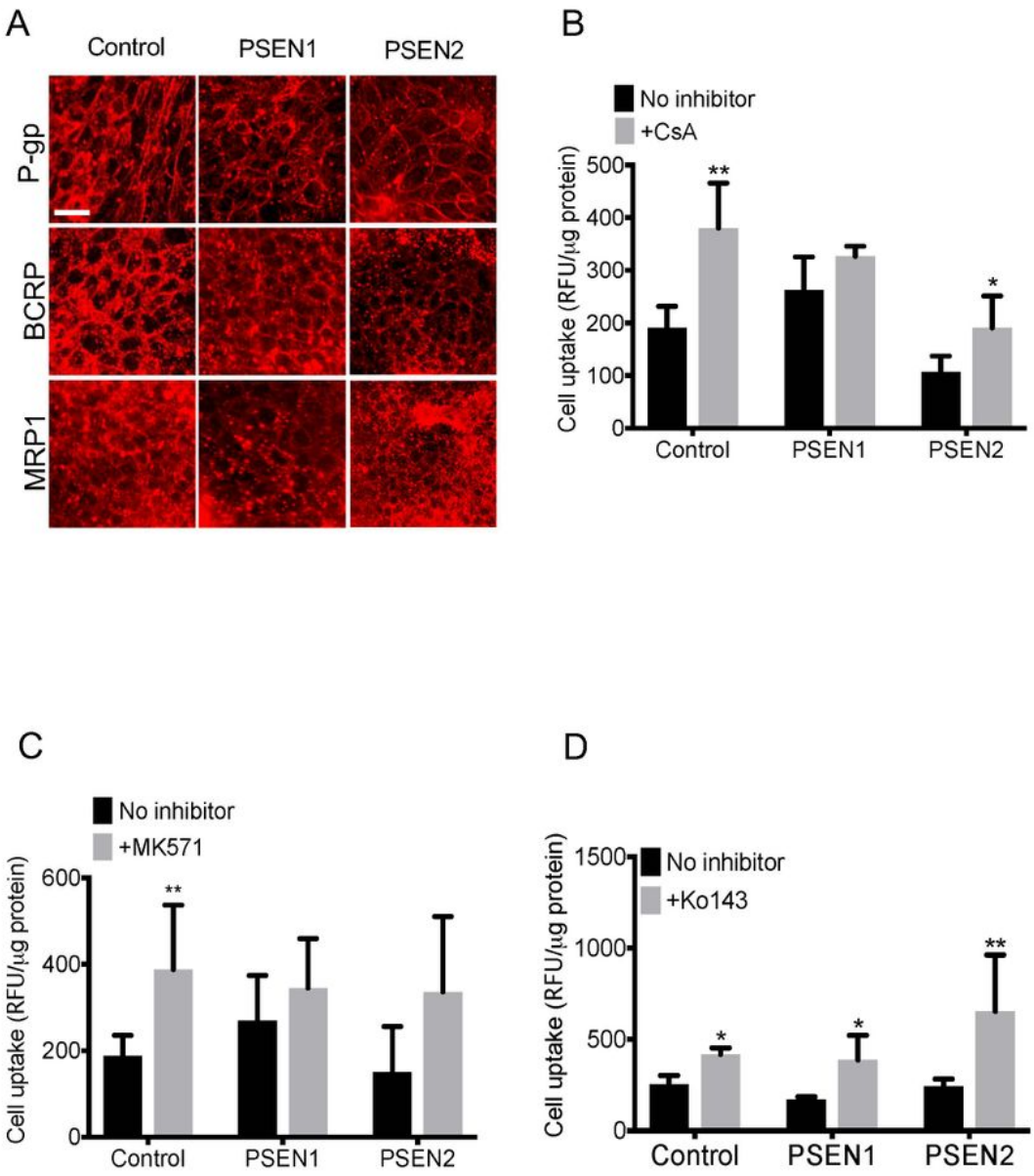

Figure 2

PSEN1-BMECs shows lower P-gp and MRP1 activity than control-BMECs and PSEN2-BMECs. (A) Representative micrograph pictures of P-gp, BCRP and MRP1 immunostaining in BMECs derived from the

control, PSEN1 and PSEN2 iPSC lines. Scale bar = 50μm. Cell uptake assay of drug efflux substrate for assessing P-gp (B), BCRP (C) and MRPs (D) activity. Note the higher P-gp and MRPs efflux substrate uptake in PSEN1-BMECs compared to the two other iPSC lines, as well as an absence of increased of drug efflux substrate in PSEN1 following P-gp and MRPs inhibition by cyclosporine A and MK571 respectively. N=3/group, * and ** denote P<0.05 and P<0.01 respectively.

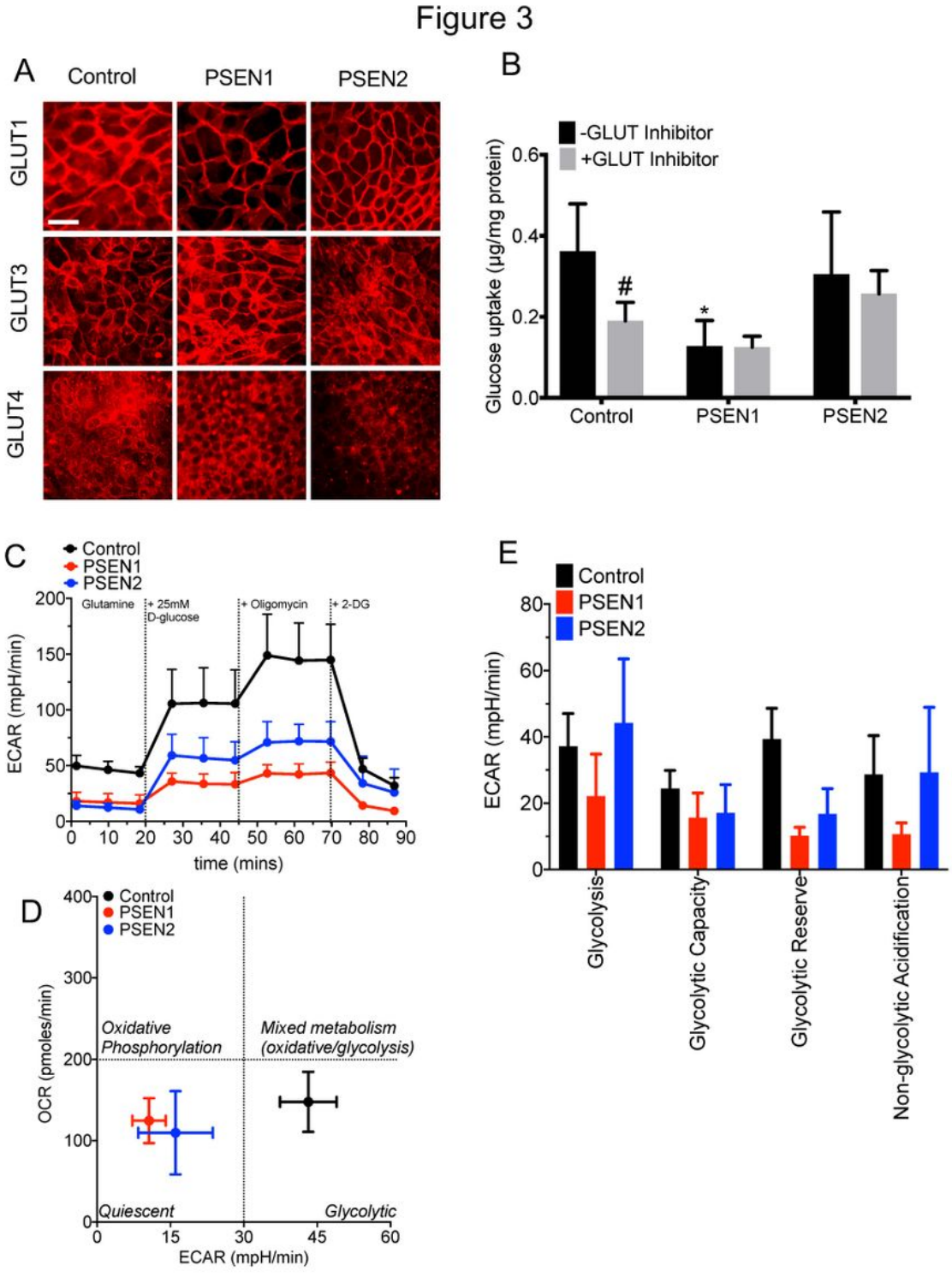

Figure 3

Effect of PSEN mutations on glucose uptake and glycolysis. (A) Representative micrograph pictures of GLUT1, GLUT3 and GLUT4 immunostaining in BMECs derived from the control, PSEN1 and PSEN2 iPSC lines. Scale bar = 50μm. (B) Glucose uptake assay in iPSC-BMECs in absence or presence of 10μM Glucose Transporter Inihibitor II. Note the absence of glucose uptake inhibition in both the PSEN1 and PSEN2 iPSC lines. (C) Glycolytic flux analysis. Representative ECAR diagram following treatment with various inhibitor. Cells were incubated for 2 hours in glucose-free medium prior onset of experiment. Cells were maintained in medium with L-glutamine, and subsequently given 10mM D-glucose, followed by incubation with 1μM oligomycin (mitochondria respiratory chain inhibitor) and 2-deoxyglucose (100mM). (D) Energy consumption profile of iPSC-BMECs. OCR denotes oxygen consumption rate, ECAR denotes extracellular acidification rate. Note the shift of metabolic activity from “glycolytic” to “quiescent” phenotype. (E) Glycolytic parameters extrapolated. Noted the lower glycolytic capacity and reserve in PSEN1 and PSEN2 iPSC-BMECss compared to control iPSC-BMECs, whereas PSEN1 showed a lower glycolysis and non-glycolytic acidification rate. N=3/group, * denotes $P<0.05$ versus control group, # denotes $P<0.05$ versus non-inhibited group.

Figure 4

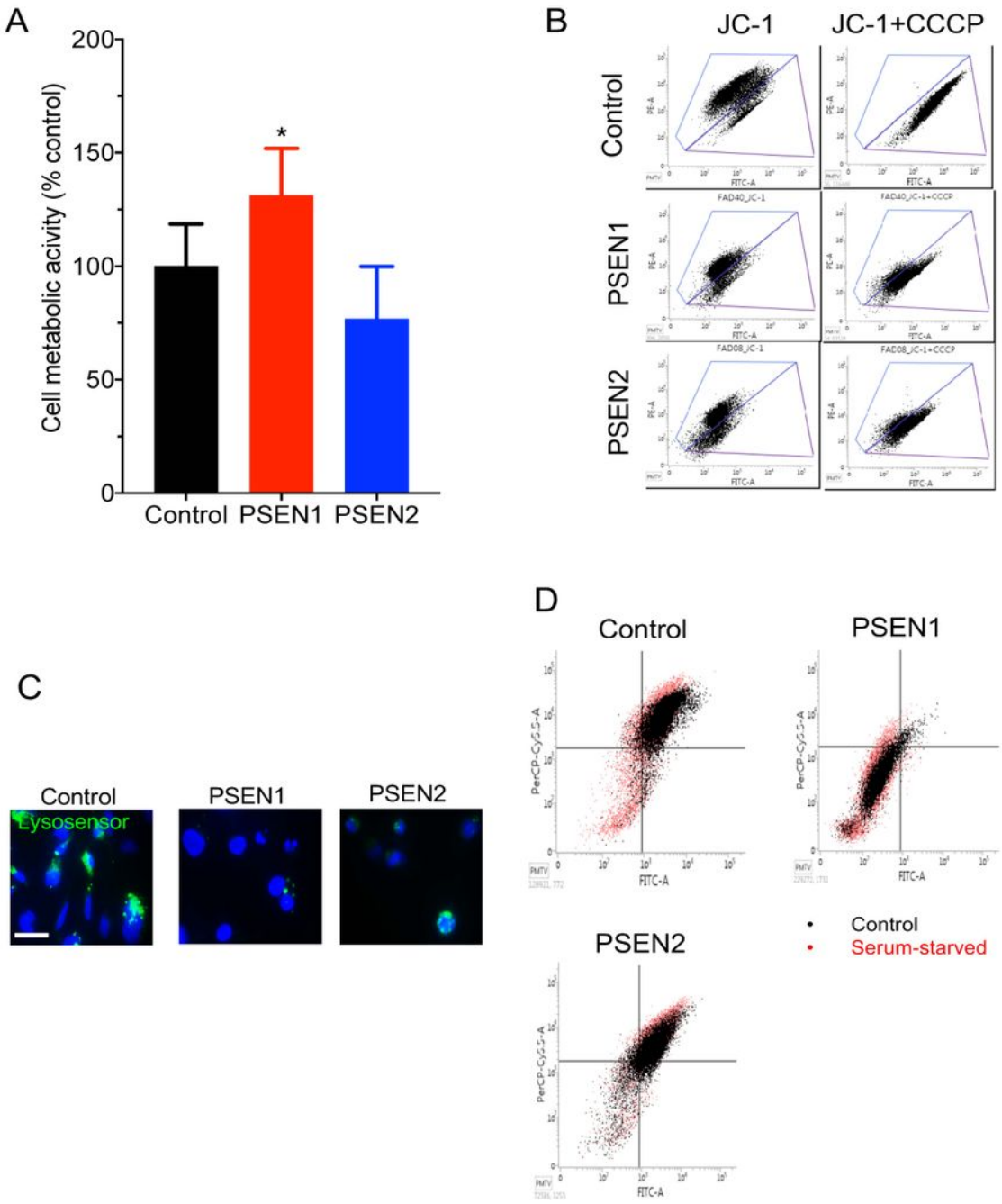

Figure 4

PSEN1 abnormally high cell metabolic activity is coupled with impaired mitochondrial function. (A) MTS assay in iPSC-derived BMECs. Cells were incubated in presence of MTS for 2 hours. MTS-conditioned medium was recovered and measured by spectrophotometry. Not the higher cell metabolic activity observed in PSEN1-BMECs compared to control-BMECs and PSEN2-BMECs. (B) JC-1 flow cytometry analysis.

Supplementary Files

This is a list of supplementary files associated with this preprint. Click to download.

- FBCNSFADBBBR0SupplFigures.pdf